RSC Advances

ROYAL SOCIETY OF CHEMISTRY

www.rsc.org/advances

Single molecular analysis of the interaction between DNA and chitosan

Yanwei Wang Xu Zhang Guangcan Yang*

School of Physics and Electronic Information, Wenzhou University, Wenzhou, 325035, China.
E-mail: yanggc@wzu.edu.cn; Fax: +86-577-86689010; Tel: +86-577-86689033

A B S T R A C T

Chitosan is a widely used potential agent for gene therapy, however its condensing process of DNA has not been fully understood. In this paper, the process is studied by atomic force microscopy (AFM) and single molecular magnetic tweezers (MT), providing direct dynamic insights of the forming process of the DNA-condensate complex. The results indicate that the polymer architecture is strongly dependent on the charge ratio of chitosan to DNA（k）, and the pH value of solution. The images of AFM show that the morphology of DNA changes from loose structures to compact ones when the charge ratio increase from 0.2 to 5. When the charge ratio is 4 and pH change from 7.4 to 8.5, the unraveling of the DNA-chitosan can be clearly observed. The compaction and unraveling of the DNA-chitosan complex are also analyzed at the single-molecule level using MT. The condensation and decondensation process has stepwise and continuous formation . The stepwise jumps in the curve may essentially reflect of the step-by-step formation of orderly toroids structures. The continuous compaction process may reflect of formation of orderly sphere and rod structures. The pulling curves contain a wide range of step sizes, ranging from tens of nanometers to few micrometers. This may reflect of other intermediate states. It is found that when the charge ratio increases from 2 to 7, the corresponding condensing forces have a linear growth of 0.5pN to 4pN, and the condensing and releasing processes are reversible. Therefore, the dominant factors in DNA condensation induced by chitosan are the charge neutralization and ion correlation effect.

Keywords: Chitosan; charge ratio; condensing force; DNA released; Atomic Force Microscoy(AFM); Magnetic Tweezers (MT)

1. Introduction

DNA condensation is a crucial process for gene therapy application since it is an important prerequisite for transporting therapeutic genes toward target cells. It is the collapse of extended

DNA chains into compact, ordered particles containing only one or a few molecules. The process can be induced by the addition of condensing agents or ligands[1]. Condensation and compaction of DNA have attracted a large amount of attention since the structures and dispensability of DNA complex have significant influence on gene transfer efficiency [2-4]. Understanding the condensation process is of interest within biotechnology and medicine for its gene therapy applications. The compacted form of DNA protects it from nucleases[5-7] and, facilitates transport through the extracellular matrix due to the reduced dimensions, and thus enhances the cellular uptake by cells through endocytosis [8]. To ensure the efficiency of therapeutic genes, the electrostatic complexation technique was selected due to its properties as a biocompatible process, requiring low energy and not using cross-linking agents [9]. The interactions between DNA and condensing agents allow DNA to undergo a dramatic condensation and compact into various structures. This is driven by the overall increase in the entropy of system due to the release of counterions[1]. The complex shows a variety of morphology, typically includes toroids, rods and globules. The relative amounts depend on many factors, such as pH in solution, charge ratios, and temperature. To overcome the electrostatic repulsion between the segments of DNA, most of its charge must be neutralized by counterions, as described in Manning's counterion condensation theory[10].

Gene therapy is a powerful treatment for curing congenital and acquired diseases which are based on the transfer of genes to the patients[11]. The major drawback of gene therapy is the transfection rate. The two main types of vectors used in gene therapy are based on viral or non-viral gene delivery systems. The viral gene delivery system shows a high transfection yield but has many disadvantages, such as oncogenic effects and immunogenicity[12]. For this reason, the development of non-viral gene delivery systems has shifted towards tailor-made polycations. These include studies of homopolymeric polycations such as poly-L-lysine (PLL)[5, 6, 13, 14] and poly(ethylenimine) (PEI)[14-17]through other cationic agents such as spermidine,[18-20] cobolthexamine, and cationic lipids to polycations produced by combinatorial chemistry. The linear copolymer chitosan has recently emerged as an attractive gene delivery vehicle because of its nontoxic and biodegradable nature[21, 22]. It is among the few candidates to report a large application potential due to its high transfection efficiency. Furthermore, DNA-chitosan complexes also have recently been reported to have high transfection efficiency, comparable to that of homopolymeric polycations [16, 22].

Chitosan, a cationic polysaccharide obtained by alkaline N-deacetylation of chitin, is one of the most widely utilized polysaccharides[22]. It is a non-toxic biodegradable polymer with low immunogenicity. These characteristics make chitosan an excellent candidate for various biomedical applications such as drug delivery, tissue engineering, and gene delivery[23-25]. It can be used for gene delivery system because positively charged chitosan can be complexed with negatively charged DNA[26-28]. In study of complexation between DNA and chitosan, a parameter k, charge ratio, is usually introduced to describe their relative concentration in solution[8]. In aqueous solution a phosphate group in DNA skeleton carries with a negative charge because of the hydration, which leads to one base pair of DNA has two element charges. On the other hand, a monomer of chitosan polymer has two amino groups positively charged two elements. The dimensionless parameter k is defined as the ratio of positive charge of chitosan to the negative charge of DNA in a unit volume. Chitosan and its derivatives have been complexed with DNA by ionic interactions between anionic phosphate backbones of DNA and primary amine groups of chitosan. This binding protects the DNA from nuclease degradation[29, 30]. Also, the mucoadhesive property of chitosan potentially permits a sustained interaction between the macromolecule[31] and the membrane epithelia, promoting more efficient uptake [28, 32]. In addition, it has the ability to open intercellular tight junctions, facilitating its transport into the cell. It has advantages of not necessitating sonication and organic solvents for its preparation, minimizing possible damage to DNA during complexation[33]. The shape dimensions of the structures[8], pH-induced DNA capture and release has also been studied[34]. Although previous studies of condensation behavior of DNA induced by chitosan have included the shape and dimensions of the structures formed at different chitosan concentration, the condensation process and the changing of the condensing force of the DNA are still unclear.

The development of the single molecule approach makes it possible for us to study the behavior of biological macromolecules under applied force; the mechanical properties of these molecules help us understand how they function in the cell [35]. Single-molecule measurements have been proven to be helpful in understanding the nucleation and growth of DNA condensates[36]. Exerting forces on DNA is a useful way to study processes relevant to DNA. The force may slow down the dynamical process so that details can be observed using an apparatus of finite temporal resolution[37].

In this paper, we used atomic force microscopy (AFM) and single-molecular magnetic tweezers (MT) methods to study the collapsing process of DNA caused by chitosan. It is found that the condensing process is related with the charge ratio of chitosan to DNA（k）and pH value of solution. From the stepwise and continuous structure of the single-molecule force spectroscopy of DNA-chitosan complex under tension, we can infer that the complexes are well organized, including toroids and rods and other intermediate states.

2. Materials and Methods

2.1 Materials

The λ-phage DNA (48502 bp，16.7μm) for MT experiment and AFM was purchased from New England Biolabs (Ipswich, MA, USA). The two ends of the DNA are singled stranded in 12 bps respectively. For the MT measurements, the λ-phage DNA were prepared by covalently attaching 12 bp chemically labeled single-stranded oligonucleotides (3'biotin-cccgccgctgga and3'digoxygenin (dig)-tccagcggcggg) to their ends according to the procedure of Smith et al[38]. Briefly, the two short oligomers are complementary to the two ends of λ DNA and they are specifically combined by adding DNA ligase and ligation buffer. Chitosan was purchased from Wako Pure Chemical industries (Deacetylation rate, min 80.0 mol%). The NH_4AC for molecular biology(≥98%) was purchased from Sigma. All agents were used as received and all experiments were repeated at least twice to ensure consistent results.

2.2 Complex Formation and Sample Preparation for AFM

Chitosan stock solution(1mg/ml) were prepared in 1% acetic acid and further diluted to the selected chitosan concentration(C_{chit})using ammonium acetate (NH_4AC,150Mm, pH 7.4). After the DNA stock solution was diluted in NH_4AC (150Mm,pH 7.4), the complexes were then prepared by adding the chitosan solution to the DNA solution, yielding a final DNA concentration(C_{DNA})of 4μg/ml with a specific k in the range between 0.1 and 7. To avoid formation of salt crystals in the dried specimens and associated obscuring effects in the images, the ammonium acetate was used instead of NaCl, to adjust the ionic strength in the solutions.

Mica pieces (about 1 cm diameter) attached to magnetic steel discs were used as substrates for DNA adsorption. Samples for AFM imaging were prepared by depositing an aliquot of 20μL of the aqueous specimen on the mica pieces and incubated for 5 minutes at room temperature.

Following incubation, samples were rinsed with a flow 20μL water solution ten times, and then the samples were dried with stream of N_2 gas and then further vacuum-dried for at least 2h. Uncomplexed DNA was immobilized on the mica surface using 3.5mM $MgCl_2$ and other measurement is under the same condition described above.

2.3 AFM Imaging and Image Analysis

An SPM-9600 atomic force microscope (Shimadzu, Kyoto, Japan) was used for imaging in the current study. All images presented here were derived from the original data and flattened to improve the contrast grade. The dried specimens were imaged in tapping mode of AFM in air, with 3 Hz scan frequency and data collection at 512×512 pixels. The extension, height, and width of the DNA in AFM imaging were measured manually using off-line analysis software equipped with the system.

2.4 Magnetic Tweezers Setup

The magnetic tweezers setup for single-molecule measurements is similar to that described by Sun et al[39]. A 0.17 mm thick coverslip with one side polished and coated with silylating reagent is sandwiched in between two glass slides. It is served as a flow chamber by sealing the open side of the structure with polydimethylsiloxane. Next, two holes with a diameter of 1 mm each were created on the top glass slide and linked with a glass capillary to facilitate buffer out or in (Fig. 1A). The polished sidewall was functionalized with antidigoxygenin to link with the dig-end of λ-DNA. The DNA molecules were first mixed with 2.8μm paramagnetic beads coated with strepavidin (M-280, Dynal Biotech) for 15 min to form bead–DNA constructs. The prepared DNA-bead constructs were dispensed into the cell to form a side wall-DNA-paramagnetic bead structure (Fig. 1B). The flow chamber is placed an inverted microscope with 40×objective. The force exerted on the beads in the focal plane is controlled by an accurately positioned permanent magnet placed lateral to the chamber. The fluctuations transverse to the pulling direction are related to the applied force by the formulae $F = K_BT\langle L\rangle/\langle \delta x^2\rangle$, where $\langle L\rangle$ is the average extension of DNA and δx is the fluctuation of the paramagnetic bead[36, 37]. The distance between the bead and the surface of the sidewall can be approximated as the extension of DNA. After a single-suspended λ-DNA was checked, the chitosan solution was loaded to the chamber. The elastic response of DNA as a function of time was recorded and analyzed at different applied forces.

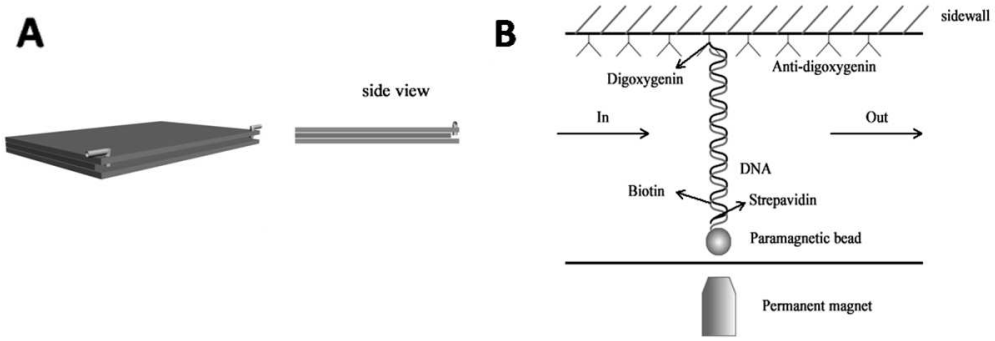

Figure1. (A) Design of flow cell. (B) Schematic diagram of magnetic tweezers.

2.5 Single-molecule measurement

In our single-molecule experiments, we pour the microsphere-bound DNA molecules into the flow cell and put the cell perpendicularly for 30 minutes at room temperature, where the polished edge surface of the cover glass is at the bottom of the cell. After the microspheres ligate the polished edge, we rinse the cell with buffer to clean out the free particles. After that we have to find a ligated particle and check whether it is connected to the surface through a single DNA molecule. Two protocols are used in the DNA pulling. In the first protocol, we pour chitosan solution at different concentrations to the flow cell, then remove the magnet so that the DNA molecule can extend with full flexibility. After incubating for 10 minutes, we increase the magnetic force gradually to determine at what force the DNA loop would open to get stretching curve . In the second protocol, we stretch the single DNA molecule to full extension, then chitosan solution is poured to the flow cell. After incubating for different times, we decrease the magnetic force gradually to determine at what force the DNA would condense to get compaction curve and the condensing force which the compaction started. In the process, the DNA extension is recorded in real-time.

3. Results and Discussion

3.1 AFM observation of DNA-chitosan complexes

In the present study, we used AFM to observe the morphologies of DNA complex adsorbed to mica surfaces in the presence of different concentration of chitosan. As described in the materials and methods section, all the uncomplexed DNA and DNA-chitosan complexes were scanned on mica surface under the condition of pH=7.4.

From the AFM images, we can see that the uncomplexed DNA molecules are fully extended and have few loops and kinks, as shown in Fig. 2A. When the charge ratio k=0.2, some local kinks appeared (Fig. 2B). We may see many loops of DNA when the charge ratio k=0.3 (Fig.2C). As k climb up to 0.5, some network structures appeared. We found that the rods and spherical structures appeared on the networks. This may give direct evidence to illustrate the forming process of the complex (Fig.2D). Meanwhile, we find these networks consisted of more than one DNA molecule, indicating that intermolecular contacts between DNA molecules were involved in the complex formation. When k goes up further, the structures become more compact and less free segments of DNA can be seen and finally disappear in the AFM images.

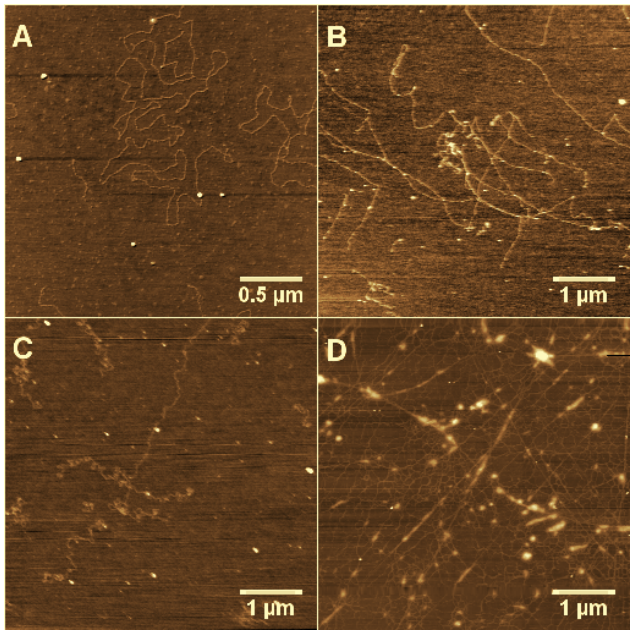

Figure2. (A) Fully extended DNA. k=0 (B) Some local links appeared, k=0.1 (C) Many loops induced by DNA kinking , k=0.3.(D) Network structures of DNA appeared, k=0.5. The final DNA concentration is 4μg/ml.

When k keeps on increasing to about 1, the morphologies of complex become dramatically different from those in the low-concentration regimes (Fig.3). When k=1,2,4 the spherical structures can be found in the Fig.3A. The rodlike structures appeared in Fig.3B and the typical toroids can be observed in the Fig.3C. In addition to the well-defined toroids and rods, other more complicated structures can be found in the image, such as those circled out in Figure 3B. From Figure 3, we can see that the size of the complexes decreases monotonously with k value, which

indicates that DNA becomes more compact since the electrostatic repulsion is overcome further by the charges neutralization of more chitosan. In other hand, the large excess of chitosan present when the complex formation takes place leads to an increased number of contact points between DNA segments and chitosan. Such numerous interactions between chitosan and DNA might result in the complexes being trapped in the intermediate states, which can be observed by AFM.

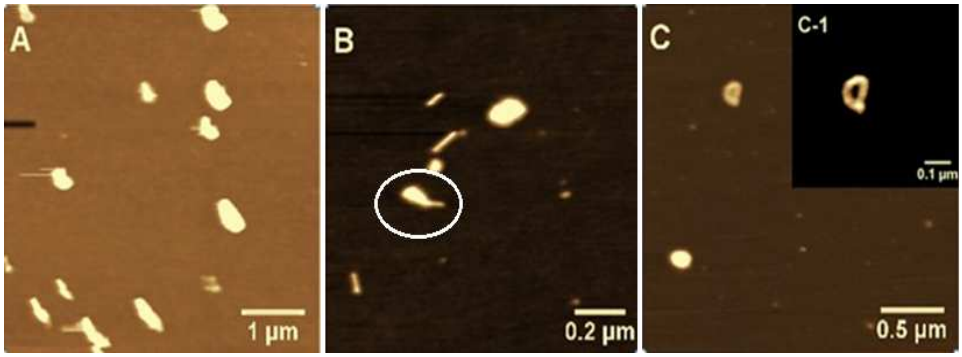

Figure3. (A) Spherical structures at k=1 . (B) Rodlike structures at k=2. (C) Toroids structure at k=4 .

As we know, The pKa of the amino functional group makes chitosan ideal for uses in DNA extraction in a manner consistent with that described for surface charge switching. Unlike polyhistidine, containing both a positively charged imidzaole group and a negatively charged carboxyl group, chitosan contains only one protonable functional moiety, resulting in a strong electrostatic interaction between chitosan and DNA at low pH or no charge at slightly higher pH[34]. Thus, with the increase of pH, the DNA will release from the DNA-chitosan complex. We changed the pH from 7.4 to 8.5 to illustrate the AFM morphology of the complex. When k=4, we found the morphology of the spherical, rod(Fig.4 A) and toroids(Fig.4 B) at pH=8.5. We found that the size of the complex were similar to that formed at pH=7.4(Fig.3 C) except the released DNA beside them. In our experiment, the spherical and rodlike structures were observed much more frequently than toroids regardless chitosan concentration. These results illustrate that the complex consisted more than one DNA molecules, indicating that intermolecular contacts between the DNA molecules were involved in the complex formation. pH might be used as a controllable DNA release approach from the condensed DNA-chitosan complexes, which is very useful in gene delivery. This observation is consistent with the result of Landers group 41. It is worth to explore further by single molecular methods.

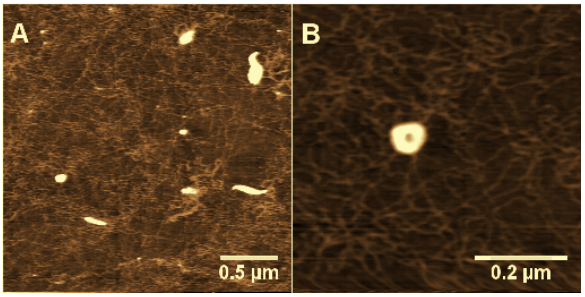

Figure4. (A) The AFM morphology of the spherical and rod. pH=8.5（k=4）. (B) The AFM morphology of toroids. pH=8.5（k=4）.

3.2 Single-molecule measurements of MT

To elucidate the dynamic process of the interaction between DNA and chitosan, we use a home-made magnetic tweezers to pull the DNA-chitosan complexes in a flow cell. In the setup afore-mentioned, a ligated bead was chosen to confirm that it was connected to the surface through a single DNA molecule, where the extension of the λ-DNA should be close to 16μm under high tension. A single DNA molecule can be picked out by matching the experimental force-extension curve to the known one of single DNA satisfying the wormlike chain model [40]. Then we flew the chitosan solution at different concentrations to the cell and stretched the DNA by moving the magnet. When we adjust the position of the magnet in the setup, we can apply adjustable force to the tethered bead. After adding chitosan, we can see the tethered DNA compaction and measure the applied force simultaneously, which is the condensing force. As the chitosan solution was loaded into the flow chamber, the tethered DNA molecule began to shrink gradually due to the condensing effects of chitosan.

Figure 5 presents typical extension-time curves at two different chitosan concentration (k=3 for A and k=4 for B), which contain the stepwise and continuous condensation structure. Before we flush chitosan into the cell, we pull single DNA chain to its full length with the applied magnetic force. When the forces are 1.26 pN and 2 pN, the corresponding extension are 14.4μm to 14.9μm respectively, shown in figure 5A and 5B. When we add the chitosan solution into the cell, the tethered DNA molecule is starting to shrink although the pulling force is still applied to the

magnetic bead. We can see that with the increase of chitosan concentration from k=3 to 4, the waiting time before the compaction occurred decreases from 1500s to 500s regardless a bigger force applied. When the compaction stopped, the final extension of DNA was also related to the exerted forces. Specifically, the paramagnetic bead came close to the sidewall of the chamber at low force（<0.5PN），whereas DNA retained an end-to-end length of 6-10μm at high force (>6PN). After condensation, the magnetic bead can be pulled back again by exerting larger forces.

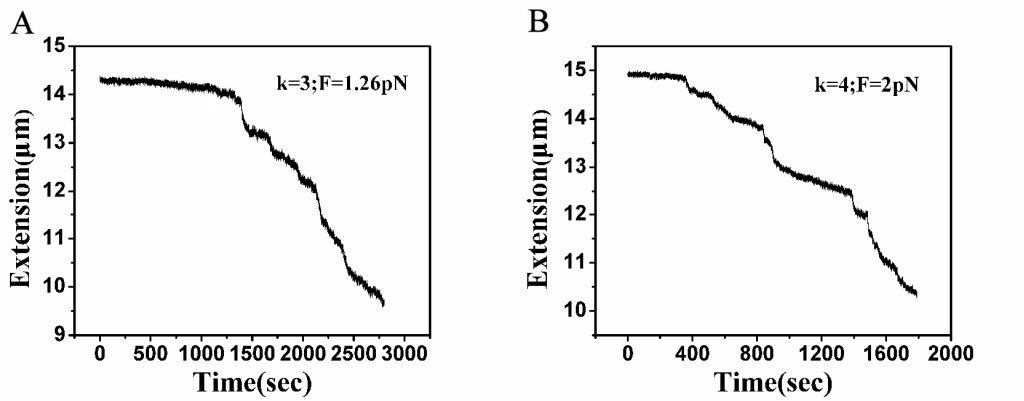

Figure5.The condensating curve of DNA induced by chitosan using magnetic tweezers at k=3(A), k=4 (B).

To study the mechanical properties of the condensing structures, we performed constant force unraveling experiments on the system. Figure 7 shows two unraveling time courses with k=3 at force 5.1PN (Fig.6A) and k=4(Fig.6B) at force 6PN. From the curves, we can see that the extension of DNA changes from 10.2μm to about 11μm in a time period about 1400 seconds. However, the applied force at k=4 is larger than that at k=3. This may be because with the increase of the k, DNA becomes more and more close-packed and the interaction between DNA and chitosan grows. With the increase of k, the force for stretching DNA to stable length obviously increased from 5.1PN to 6PN. The unraveling process contains both stepwise and continuous processes depending on chitosan concentrations.

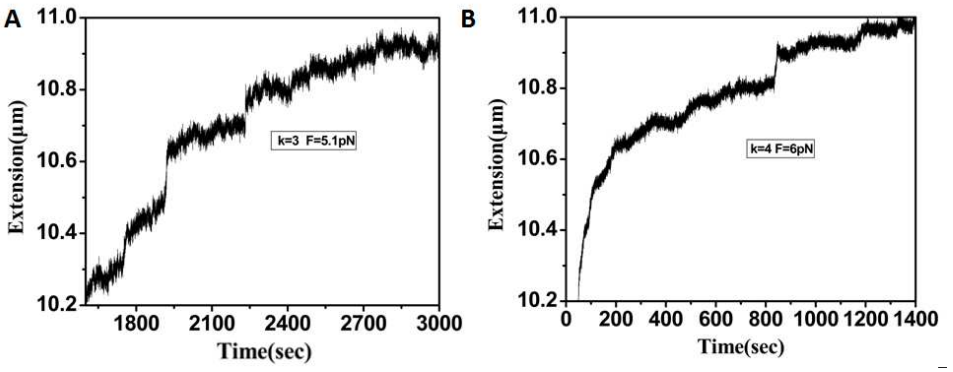

Figure6. The unraveling curve of condensate DNA induced by chitosan using magnetic tweezers, when k=3(A), 4(B).

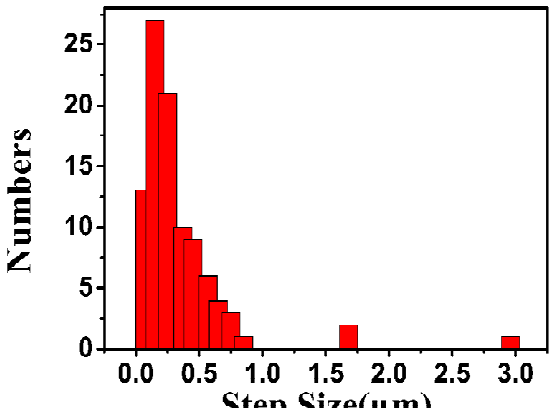

Figure7. The statistics of DNA step size induced by chitosan at all of the k.

We can notice a series of stepwise jumps in both condensing and unraveling processes at different chitosan concentrations. The statistics of the step sizes are shown in figure 7, where 100 steps in both compacting and unraveling curves are used. The distribution peak in the frequency histogram occurs at a typical size 0.25μm although some bigger step sizes up to 3μm also can be observed. The step sizes observed in our experiments are similar to the results that were induced by multivalent cations, indicated that typical toroids was the main structure in the complex.[37] .

The condensation and decondensation process have stepwise and continuous patterns. The stepwise jumps in the curves may essentially reflect of the step-by-step formation of orderly toroids structures. The continuous compaction process may reflect of formation of orderly sphere and rod structures. The big steps in figure 7 may involve of pulling open the complexes being

trapped in intermediate states or more than one turns of DNA were unwrapped from the toroids at the same time. In addition, the concentration dependence in the compaction and decompaction processes demonstrates that high chitosan concentration helps overcome the energy barrier and stabilize the compact complex.

From the pulling curves of DNA in chitosan solution with different k, we can obtain more insights of the condensing process and its dynamics. In order to get more accurate condensing forces under the different chitosan concentration, we made the statistics for cohesion under k = 2, 3, 4 and 7 shown in figure 8. At each concentration, 20 samples were used for statistics. We can see that the distribution of condensing force is rather scattered from 0.5 pN to about 8 pN, but has a statistical peak for each concentration. The position of peak moves up when the corresponding concentration of chitosan grows. When k=2, shown in Fig. 8A, we can see that condensing forces are mainly distributed between 0 and 1 pN, but can reach as high as 3.5 PN. When k = 3(Fig.8B), most of the condensing forces are located between 1 and 1.5 PN though some forces can arrive 4.5 PN. When we increase the concentration of chitosan further, similar distribution can be observed, which are shown in Fig. 8C and 8D. It is found that when the charge ratio increases from 2 to 7, the corresponding condensing force peak moves from 0.5pN to 4pN. We can conclude that DNA become more and more close-packed and the interaction between DNA and chitosan becomes stronger with the increasing k. This conclusion can be confirmed by the AFM images of DNA-chitosan complex. We can see that the dimension of complex decreased when k increases.

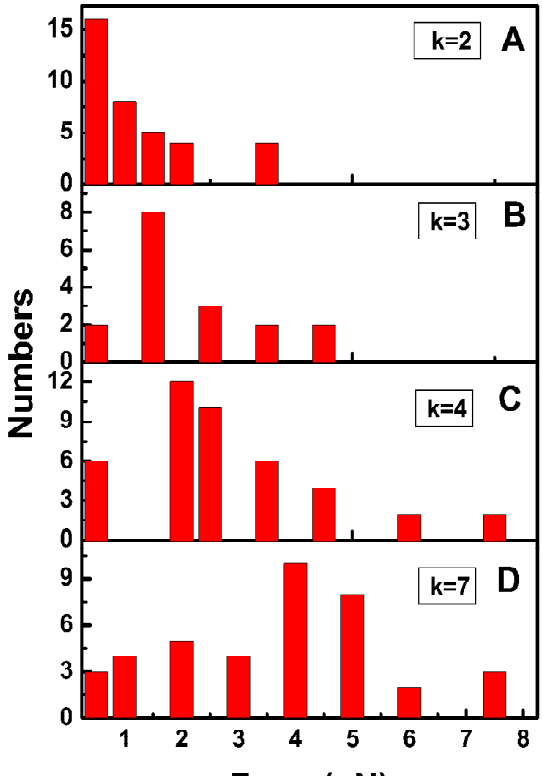

Figure8. The statistics of condensing force, when k=2, 3, 4, 7

4. Conclusion

In summary, the compaction of DNA induced by chitosan has been studied using AFM scanning method and MT. This study demonstrates that chitosan effectively condense DNA into toroidal, rodlike or other structures with the dominating topology depending on k. The strength of the intersegment interaction, mediated by the charge of the chitosan, is important in determining the shape of the DNA-chitosan complexes.

The formation and unraveling processes of DNA-chitosan complex displayed stepwise and continuous formation, indicating that the complexes are well organized toroids and rods states or other intermediate states. The stepwise jumps in the curve may essentially reflect of the step-by-step formation of orderly toroids structures. The continuous compaction process may reflect of formation of orderly sphere and rod structures. It is found that when the charge ratio increase from 2 to 7, the corresponding condensing forces have a linear growth of 0.5pN to 4pN, and the condensing and releasing processes are reversible.

Acknowledgments

The project was supported by the National Natural Science Foundation of China (11274245, 10974146, 11304232) and Zhejiang Provincial Natural Science Foundation (Y6090222).

References

1. V. A. Bloomfield, *Current opinion in structural biology*, 1996, **6**, 334-341.
2. J. Pelta, D. Durand, J. Doucet and F. Livolant, *Biophysical journal*, 1996, **71**, 48-63.
3. E. Raspaud, D. Durand and F. Livolant, *Biophysical journal*, 2005, **88**, 392-403.
4. N. V. Hud and I. D. Vilfan, *Annual Review of Biophysics and Biomolecular Structure*, 2005, **34**, 295-318.
5. B. Zhang and S. Mallapragada, *Acta Biomaterialia*, 2011, **7**, 1570-1579.
6. A. Qi, P. Chan, J. Ho, A. Rajapaksa, J. Friend and L. Yeo, *ACS nano*, 2011, **5**, 9583-9591.
7. J. Malmo, K. M. Vårum and S. P. Strand, *Biomacromolecules*, 2011, **12**, 721-729.
8. S. Danielsen, K. M. Vårum and B. T. Stokke, *Biomacromolecules*, 2004, **5**, 928-936.
9. S. Lankalapalli and V. Kolapalli, *Indian journal of pharmaceutical sciences*, 2009, **71**, 481.
10. V. A. Bloomfield, *Biopolymers*, 1997, **44**, 269-282.
11. C. Aral and J. Akbuga, *J Pharm Pharm Sci*, 2003, **6**, 321-326.
12. S. Mansouri, P. Lavigne, K. Corsi, M. Benderdour, E. Beaumont and J. C. Fernandes, *European Journal of Pharmaceutics and Biopharmaceutics*, 2004, **57**, 1-8.
13. P. L. Ma, M. D. Buschmann and F. M. Winnik, *Analytical chemistry*, 2010, **82**, 9636-9643.
14. M. Alatorre-Meda, P. Taboada, F. Hartl, T. Wagner, M. Freis and J. R. Rodríguez, *Colloids and Surfaces B: Biointerfaces*, 2011, **82**, 54-62.
15. J. H. Yu, J. Huang, J. W. Nah, M. H. Cho and C. S. Cho, *Journal of Applied Polymer Science*, 2009, **115**, 1189-1198.
16. C. Narambuena, E. Leiva, M. Chávez-Páez and E. Pérez, *Polymer*, 2010, **51**, 3293-3302.
17. J. J. Thomas, M. Rekha and C. P. Sharma, *Colloids and Surfaces B: Biointerfaces*, 2010, **81**, 195-205.
18. W. Zhang, S. Pan, Y. Wen, X. Luo and X. Zhang, *Journal of Biomaterials Science, Polymer Edition*, 2010, **21**, 741-758.
19. G. Puras, J. Zarate, M. Aceves, A. Murua, A. Díaz, M. AvilésTriguero, E. Fernández and J. Pedraz, *European Journal of Pharmaceutics and Biopharmaceutics*, 2013, **83**, 131-140.
20. E. Talvitie, J. Leppiniemi, A. Mikhailov, V. P. Hytönen and M. Kellomäki, *Carbohydrate Polymers*, 2012, 948–954.
21. M. Alatorre-Meda, P. Taboada, J. Sabín, B. Krajewska, L. M. Varela and J. R. Rodríguez, *Colloids and Surfaces A: Physicochemical and Engineering Aspects*, 2009, **339**, 145-152.
22. V. Ivanov, J. Martemyanova, M. Muller, W. Paul and K. Binder, *The Journal of Physical Chemistry B*, 2008, **113**, 3653-3668.
23. E. Salas, P. Martinez, R. Godinez, A. A. Del Nunez and C. Miranda, *Asian Chitin Journal*, 2008, **4**, 59-66.
24. R. Jayakumar, N. Nwe, S. Tokura and H. Tamura, *International Journal of Biological Macromolecules*, 2007, **40**, 175-181.
25. E. Kai and T. Ochiya, *Pharmaceutical research*, 2004, **21**, 838-843.
26. F. C. MacLaughlin, R. J. Mumper, J. Wang, J. M. Tagliaferri, I. Gill, M. Hinchcliffe and A. P. Rolland, *Journal of controlled release*, 1998, **56**, 259-272.
27. N. Fang, V. Chan, H.-Q. Mao and K. W. Leong, *Biomacromolecules*, 2001, **2**, 1161-1168.

28. S. W. Richardson, H. J. Kolbe and R. Duncan, *International journal of pharmaceutics*, 1999, **178**, 231-243.
29. Z. Cui and R. J. Mumper, *Journal of controlled release*, 2001, **75**, 409-419.
30. L. Illum, I. Jabbal-Gill, M. Hinchcliffe, A. Fisher and S. Davis, *Advanced drug delivery reviews*, 2001, **51**, 81-96.
31. S. Özbaş-Turan, J. Akbuğa and C. Aral, *Journal of pharmaceutical sciences*, 2002, **91**, 1245-1251.
32. R. Hejazi and M. Amiji, *Journal of controlled release*, 2003, **89**, 151-165.
33. R. Jayakumar, K. Chennazhi, R. Muzzarelli, H. Tamura, S. Nair and N. Selvamurugan, *Carbohydrate Polymers*, 2010, **79**, 1-8.
34. W. Cao, C. J. Easley, J. P. Ferrance and J. P. Landers, *Analytical chemistry*, 2006, **78**, 7222-7228.
35. Y. Wang, S. Ran, B. Man and G. Yang, *Soft Matter,* 2011, **7**, 4425.
36. S. Y. Ran, Y. W. Wang, G. C. Yang and L. X. Zhang, *The Journal of Physical Chemistry B*, 2011, **115**, 4568-4575.
37. W. B. Fu, X. L. Wang, X. H. Zhang, S. Y. Ran, J. Yan and M. Li, *Journal of the American Chemical Society*, 2006, **128**, 15040-15041.
38. S. B.Smith, L. Finzi, C. Bustamante, S*cience*, 1992, **258**, 1122.
39. B. Sun, K. J. Wei, B. Zhang, X. H. Zhang, S. X. Dou, M. Li and X. G. Xi, *The EMBO journal*, 2008, **27**, 3279-3287.
40. J. F. Marko , E. D. Siggia, *Macromolecules*, 1995, *28* (26), ,8759–8770
41. W. Cao, C. J. Easley, J. P. Ferrance and J. P. Landers, *Analytical chemistry*, 2006, **78**, 7222-7228.